Lyapunov-Based Control Scheme for Single-Phase Grid-Connected PV Central Inverters

Meza, C.; Biel, D.; Jeltsema, D.; Scherpen, J. M. A.

Published in:
IEEE Transactions on Control Systems Technology

DOI:
10.1109/TCST.2011.2114348

Publication date:
2012

Lyapunov-Based Control Scheme for Single-Phase Grid-Connected PV Central Inverters

C. Meza, *Member, IEEE,* D. Biel, *Member, IEEE,* D. Jeltsema, *Member, IEEE,* and J. Scherpen, *Senior Member, IEEE*

Abstract

A Lyapunov-based control scheme for single-phase single-stage grid-connected photovoltaic central inverters is presented. Besides rendering the closed-loop system globally stable the designed controller is able to deal with the system uncertainty that depends on the solar irradiance. A set of experimental results carried out on a laboratory prototype is provided to test the proposed approach in a realisitc environment.

C. Meza is with the Electronic Engineering School, Costa Rica Institute of Technology, Cartago, Costa Rica, E-mail: cmeza@ietec.org

D. Biel is with the Institute of Industrial and Control Engineering, UPC, Barcelona, Spain, E-mail: biel@eel.upc.edu

D. Jeltsema is with Delft Institute of Applied Mathematics, Delft University of Technology, E-mail: d.jeltsema@tudelft.nl

J. Scherpen is with Discrete Technology and Production Automation, University of Groningen, E-mail: j.m.a.scherpen@rug.nl

Lyapunov-Based Control Scheme for Single-Phase Grid-Connected PV Central Inverters

I. Introduction

THE inconveniences related to conventional energy generation have motivated the introduction of new regulations created to stimulate the usage of photovoltaic (PV) systems. The success of these policies relies on the cost-per-watt reduction of PV systems in order to make the PV energy more competitive with respect to traditional energy sources. In general, current research to reduce the cost-per-watt of PV systems includes:

1) improving the efficiency of PV cells/modules;
2) reducing the manufacturing costs of PV cells/modules;
3) increasing the overall PV system efficiency by focusing on the power conditioning elements.

During the last years a lot of effort has been devoted to the first two aforementioned activities, yielding high-efficient and cheaper PV panels based on new PV cell material and manufacturing technologies. An alternative way to reduce the cost-per-watt of existing PV systems is by increasing the efficiency of the overall system using a suitable designed power conditioning stage. The power conditioning stage is an essential part of the PV system since it must account for an optimal energy transfer from the energy source to the load. Improving the quality of the power conditioning stage is one of the key issues of future PV applications [1].

The design of a PV power conditioning system generally consists of a two step procedure, namely, (i) a proper selection of the circuit topology and the elements of the power converter, and (ii) the design of an adequate control strategy for the chosen power conditioning stage. The latter task is important when aiming at a stable non-oscillatory dynamical behavior of the PV system. Regarding the design of control strategies for power converters it is evident that there is a long tradition of using linear design techniques. Linear controllers are found suitable in those cases where the power converter operates about a fixed operating point and the disturbances are small. The control of power inverters and rectifiers in order to obtain a sinusoidal current in phase with the grid voltage have mainly been done by means of the so-called “P+Resonant” controllers. For a linear system, e.g., a battery inverter, it is possible to show by means of the internal mode principle that there exists a linear transfer function capable of eliminating the steady-state error ([2], [3]).

P+Resonant controllers have also been used to control the output inverter stage of multi-stage grid-connected PV systems. In this case, the adequate dimensioning of the DC link capacitor allows to approximate the output inverter stage as a linear system independent of the PV array non-linear characteristics, and therefore apply the “P+Resonant” controller design procedure [3], [4].

Nevertheless, for single-phase grid-connected PV inverters the use of linear techniques, such as Laplace transformations or frequency-based analysis, is not possible since (i) the PV source exhibits a strongly non-linear electrical behavior that affects all the variables of the system, and (ii) the electrical characteristics of the PV source are time-varying and therefore the system

is not linearizable around a unique operating point or trajectory. These difficulties have motivated us to proceed with a different approach than the usual “classical” control techniques. Moreover, for similar reasons as discussed above, there is a growing interest in the context of non-linear control of power converters from researchers of both the power electronics and the control community, see e.g., [5], [6], [7], and [8]. Of special interest is the Lyapunov-based non-linear controller technique for power converters proposed in [9] that renders the closed-loop system globally asymptotically stable. This technique has been proved useful for DC-DC converters (e.g. [10]) and AC-DC converters (e.g. [11]). In the context of PV power systems, [12] presents a globally stable closed-loop system for a single-stage full-bridge grid-connected power inverter using a similar controller design technique than that of [9]. Some disadvantages of non-linear controllers for power converters that may be encountered during the practical implementation are the computational complexity and its dependency on the system’s parameters. Nevertheless, the high processing power normally required by non-linear controllers is not a serious problem given the recent development of new processors with increase performance at reasonable prices. On the other hand, there are cases (e.g., [13] and [14]) in which the parameter dependency of the non-linear controllers has been circumvented adding an adaptive functionality to the control scheme

This paper introduces a non-linear and adaptive control scheme for a single-phase single-stage grid-connected PV inverter. It is shown by means of an analytical and experimental study that the proposed controller provides a satisfactory closed-loop behavior without neglecting the non-linear electrical characteristics of the system. The main contribution of this paper consists in extending the robustness of the controller proposed in [12] by estimating the value of the parameter that changes with the unknown solar irradiance. Additionally, the practical validity of the proposed control scheme is evaluated using an experimental laboratory prototype.

II. Grid-Connected PV System

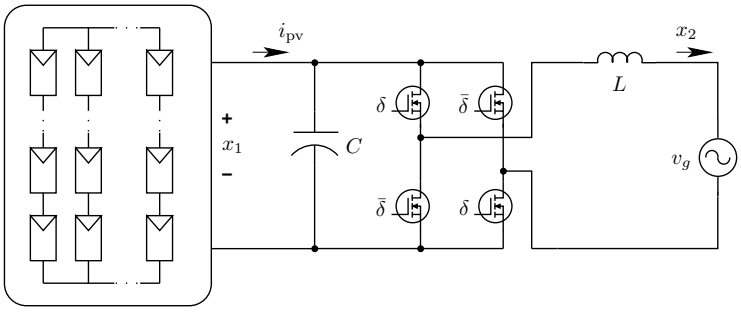

Fig. 1: Full-bridge grid-connected PV inverter schematic.

The grid-connected Photovoltaic (GPV) system that is considered in the present paper is shown in Fig. 1. The system consists of an array of PV panels connected to the utility grid by means of a full-bridge inverter. This configuration in which all the PV panels are linked to a unique power inverter unit is known as “central inverter”. A grid-connected PV system based on a central inverter is one of the most prevailing configurations since, under uniform irradiance conditions of the PV panels, it represents a good trade-off between the extracted energy and the design complexity of the power inverter [15], [16], [17]. Moreover, the full-bridge power inverter stage is a typical output stage present in other GPV configurations such as the widely

used two-stage boost-buck configuration (e.g., [18], [19]) or the multilevel configuration (e.g., [20]). As stated in [21], this common output stage enables to extrapolate the central inverter's control scheme to other configurations.

A. PV Generator

The typical electrical behavior of a c-Si PV cell can be modeled in the following way

$$i_{\mathrm{pv_{cell}}} = I_{\mathrm{g_{cell}}} - I_{\mathrm{sat_{cell}}} \left[\exp\left(\frac{v_{\mathrm{pv_{cell}}}}{\eta v_{\mathrm{T_{cell}}}} \right) - 1 \right], \tag{1}$$

where $i_{\mathrm{pv_{cell}}}$ and $v_{\mathrm{pv_{cell}}}$ are the cell current and voltage, respectively, and

- $I_{\mathrm{g_{cell}}}(G)$ is the generated current due to the incident solar irradiance G,
- η is the PV cell emission coefficient,
- $I_{\mathrm{sat_{cell}}}(T)$ is the reverse saturation current of the PV cell p-n junction that varies with the temperature T,
- $v_{T_{\mathrm{cell}}}(T)$ is the p-n junction thermal voltage which also changes with the temperature.

Given that PV cells are usually located in an uncontrolled atmospheric environment they are exposed to temperature (T) and solar irradiance (G) variations and rigorously $I_{\mathrm{g_{cell}}}(t)$, $I_{\mathrm{sat_{cell}}}(t)$, and $v_{T_{\mathrm{cell}}}(t)$ should be considered as time-varying signals. Note also that, for the case of c-Si solar cells, it is possible to derivate mathematical expressions to obtain accurately its parameters at any moment providing temperature and solar irradiance measurements [22], [23], [24]. Nonetheless, differently from temperature sensors, solar irradiance sensors are costly and difficult to calibrate properly. Accordingly, in the present paper we assume that the parameters that depend on temperature are known.

For analytical convenience we assume that the electrical behavior of a PV array is defined as follows

$$i_{\mathrm{pv}} = \Lambda - \rho(v_{\mathrm{pv}}), \tag{2}$$

where v_{pv} and i_{pv} are the PV array voltage and current, respectively, and Λ represents the part of the photovoltaic generator current that depends on the time-varying solar irradiance. The last term of (2) denotes the direct link between the voltage of the photovoltaic generator and the associated current, i.e.,

$$\rho(v_{\mathrm{pv}}) = \Psi \exp\left(\alpha\, v_{\mathrm{pv}}\right), \tag{3}$$

where Ψ and α represent positive parameters of the photovoltaic generator. Referring to the equation of the PV cell (1), the parameters Λ, Ψ and α can be defined as follows:

$$\begin{aligned} \Lambda &= (I_{\mathrm{g_{cell}}} + I_{\mathrm{sat_{cell}}}) n_p \\ \Psi &= I_{\mathrm{sat_{cell}}}\, n_p \\ \alpha &= \frac{n_s}{\eta v_{T_{\mathrm{cell}}}}, \end{aligned}$$

where n_s and n_p are the number of PV cells connected in series and parallel, respectively.

B. Power Conditioning System

The schematic diagram of the full-bridge central inverter configuration is shown in Fig. 1. Here x_1 and x_2 are the average values of the input capacitor voltage and the output inductor current, respectively. The utility grid voltage v_g is assumed to be sinusoidal with a constant amplitude A and a constant frequency ω, i.e., $v_g = A\sin(\omega t)$. The full-bridge inverter consists of four switches controlled by the signals δ and $\bar{\delta}$ which take values in the discrete set $\{0, 1\}$ (i.e., OFF or ON, respectively). The switch control signals are generated via a pulse-width modulation (PWM) scheme with a duty ratio function $u \in [-1, 1]$ generated by the controller. This means that if the switching frequency is sufficiently high, the dynamical behavior of the GPV system can be approximated by the following set of differential equations

$$\begin{aligned} C\dot{x}_1 &= -u\,x_2 + \Lambda - \rho(x_1) \\ L\dot{x}_2 &= u\,x_1 - v_g. \end{aligned} \tag{4}$$

The latter equations will be used to design a controller for the system, where we assume that the only unknown time-varying parameter is Λ. The controller should be able to deal with this parameter uncertainty.

III. Controller Design

A. Control Objectives

The main control objectives are that the grid-connected PV system should

C1. deliver a sinusoidal current in phase with the utility voltage of the power grid;

C2. regulate the input capacitor voltage to a value that assures maximum power extraction from the PV array.

B. Proposed Controller

In order to obtain an implementable non-linear control law the controller design methodology is divided in two parts, namely,

P1. an *analytical* control design stage in which a globally-stable closed-loop system is obtained based on the nonlinear model of the system, and

P2. a *practical* control design stage in which practical aspects of the system are considered, e.g., the controller derived is adapted to be implemented experimentally, and a robustness analysis is performed to assure the adequate closed-loop behavior under parameter uncertainties.

The proposed control scheme is based on the work of [9]. This controller design technique is successfully applied to power converters with constant energy sources under the assumption that all the system parameters are known (see e.g., [10] for DC-DC power converter applications and [11] for AC-DC power converter applications). The novelty of the control scheme presented in this paper lies in the extension of the control strategy of [9] in order to deal with the PV inverter's non-linear energy source characteristics and the uncertainty of the time-varying parameter Λ. Additionally, the robustness of the proposed control scheme to various parameter uncertainties in the system is considered.

Following [9], we will start the control scheme design by defining an adequate reference system for the GPV inverter under consideration, i.e.,

$$\begin{aligned} C\dot{x}_{1\mathrm{r}} &= -u_{\mathrm{r}}\, x_{2\mathrm{r}} + \hat{\Lambda} - \rho(x_{1\mathrm{r}}) \\ L\dot{x}_{2\mathrm{r}} &= u_{\mathrm{r}}\, x_{1\mathrm{r}} - v_g, \end{aligned} \tag{5}$$

where ideally $x_{1\mathrm{r}}$ and $x_{2\mathrm{r}}$ are the desired capacitor voltage and the output current, respectively, and $\hat{\Lambda}$ is the estimated value of Λ.

Notice that $x_{1\mathrm{r}}$ and $x_{2\mathrm{r}}$ cannot be defined separately since there exists a mutual dependence between them. Indeed, from (5) it can be derived an expression that relates $x_{1\mathrm{r}}$ and $x_{2\mathrm{r}}$ independently from u_{r}, i.e.,

$$x_{1\mathrm{r}} C\dot{x}_{1\mathrm{r}} + x_{2\mathrm{r}} L\dot{x}_{2\mathrm{r}} = \hat{\Lambda} x_{1\mathrm{r}} - x_{1\mathrm{r}}\rho(x_{1\mathrm{r}}) - v_g x_{2\mathrm{r}}. \tag{6}$$

Setting $x_{2\mathrm{r}}$ to be proportional to the utility grid voltage (control objective C.1), i.e.,

$$x_{2\mathrm{r}} = A_{\mathrm{Ir}} \sin(\omega t), \tag{7}$$

where A_{Ir} is the amplitude of the reference current, it is possible to obtain an expression for $x_{1\mathrm{r}}$ from (6). Similarly, signal u_{r} is obtained from (5), i.e.,

$$u_{\mathrm{r}} = \frac{L\dot{x}_{2\mathrm{r}} + v_g}{x_{1\mathrm{r}}}. \tag{8}$$

Now, let $\tilde{x}_1$, $\tilde{x}_2$, $\tilde{u}$, and $\tilde{\Lambda}$ represent the errors between the actual measured variables and their reference counterparts, i.e., $\tilde{x}_1 = x_1 - x_{1\mathrm{r}}$, $\tilde{x}_2 = x_2 - x_{2\mathrm{r}}$, $\tilde{u} = u - u_{\mathrm{r}}$, and $\tilde{\Lambda} = \Lambda - \hat{\Lambda}$, respectively, then the system dynamics can be written as

$$\begin{aligned} C\big(\dot{\tilde{x}}_1 + \dot{x}_{1\mathrm{r}}\big) &= -\big(\tilde{u} + u_{\mathrm{r}}\big)\big(\tilde{x}_2 + x_{2\mathrm{r}}\big) + \\ &\qquad \tilde{\Lambda} + \hat{\Lambda} - \rho(x_{1\mathrm{r}}) - \tilde{\rho}(\tilde{x}_1, x_{1\mathrm{r}}) \\ L\big(\dot{\tilde{x}}_2 + \dot{x}_{2\mathrm{r}}\big) &= \big(\tilde{u} + u_{\mathrm{r}}\big)\big(\tilde{x}_1 + x_{1\mathrm{r}}\big) - v_{\mathrm{g}}, \end{aligned} \tag{9}$$

where $\rho(x_1)$ is decomposed into

$$\rho(x_1) = \rho(x_{1\mathrm{r}}) + \tilde{\rho}(\tilde{x}_1, x_{1\mathrm{r}})$$

with

$$\tilde{\rho}(\tilde{x}_1, x_{1\mathrm{r}}) = \Psi[\exp(\alpha\tilde{x}_1 + \alpha x_{1\mathrm{r}}) - \exp(\alpha x_{1\mathrm{r}})].$$

According to [9] it is possible to synthesize a control signal that yields the desired closed loop behavior from the system error dynamics. In this regard, the control signal u is composed of two elements, namely, a control u_{r} defined according to (8) and a control $\tilde{u}$ designed such that the system error dynamics vanishes. The error dynamics are obtained by substituting (5) in (9), i.e.,

$$\begin{aligned} C\dot{\tilde{x}}_1 &= -u_{\mathrm{r}}\, \tilde{x}_2 - \tilde{u}\,(x_{2\mathrm{r}} + \tilde{x}_2) + \tilde{\Lambda} - \tilde{\rho}(\tilde{x}_1, x_{1\mathrm{r}}) \\ L\dot{\tilde{x}}_2 &= u_r\, \tilde{x}_1 + \tilde{u}\,(x_{1\mathrm{r}} + \tilde{x}_1). \end{aligned} \tag{10}$$

Notice that in our case we do not only have to synthesize the control $\tilde{u}$ that renders the error dynamics (10) stable, but we should derive an additional mechanism to estimate parameter Λ, i.e., to make $\hat{\Lambda} = \Lambda$. In this regard, in order to proof the validity of our control scheme the final stability analysis should take into account the designed signal $\tilde{u}$ and the dynamics associated to the estimation of Λ.

In order to estimate $\hat{\Lambda}$, the following adaptive law, taken from [14], is used

$$\dot{\hat{\Lambda}} = \mathsf{Prj}\{\gamma\, \tilde{x}_1\} = \begin{cases} \gamma \tilde{x}_1 & \text{if } \hat{\Lambda} > \epsilon \\ 0 & \text{otherwise} \end{cases} \tag{11}$$

where $\gamma \in \mathbb{R}^+$ is the adaptive gain and $\mathsf{Prj}\{\cdot\}$ is a projection operator that ensures $\hat{\Lambda} \geq \epsilon > 0$, with ϵ an arbitrary small constant.

The stability of the error dynamics (10) can be proved by means of the following Lyapunov function

$$H = \frac{1}{2} C \tilde{x}_1^2 + \frac{1}{2} L \tilde{x}_2^2 + \frac{1}{2\gamma} \tilde{\Lambda}^2, \tag{12}$$

for which the time derivative along the system trajectories of (10) yields

$$\dot{H} = \tilde{u}\,(x_{1\mathrm{r}} \tilde{x}_2 - x_{2\mathrm{r}} \tilde{x}_1) - \tilde{x}_1 \tilde{\rho}(\tilde{x}_1, x_{1\mathrm{r}}) + \tilde{\Lambda} \tilde{x}_1 + \frac{1}{\gamma} \tilde{\Lambda} \dot{\tilde{\Lambda}}. \tag{13}$$

The closed-loop system will be globally asymptotically stable if the aforementioned expression is negative definite, i.e., if $\dot{H} < 0$ for all values of $\tilde{x}_1$, $\tilde{x}_2$, $\tilde{\Lambda}$ different from zero.

Defining $\tilde{u}$ as

$$\tilde{u} = -K(x_{1\mathrm{r}}\, \tilde{x}_2 - x_{2\mathrm{r}}\, \tilde{x}_1), \tag{14}$$

where $K > 0$ is a control parameter, the first term of (13) remains always non-positive, i.e.,

$$\dot{H} = -K\,(x_{1\mathrm{r}} \tilde{x}_2 - x_{2\mathrm{r}} \tilde{x}_1)^2 - \tilde{x}_1 \tilde{\rho}(\tilde{x}_1, x_{1\mathrm{r}}) + \tilde{\Lambda} \tilde{x}_1 + \frac{1}{\gamma} \tilde{\Lambda} \dot{\tilde{\Lambda}}. \tag{15}$$

On the other hand, considering Λ "locally constant", yields

$$\dot{\tilde{\Lambda}} = -\dot{\hat{\Lambda}},$$

and according to (11),

$$\dot{\tilde{\Lambda}} = -\gamma\, \tilde{x_1}, \tag{16}$$

and thus, the derivative of the Lyapunov function (15) can be written as

$$\dot{H} = -K\,(x_{1\mathrm{r}} \tilde{x}_2 - x_{2r} \tilde{x}_1)^2 - \tilde{x}_1 \tilde{\rho}(\tilde{x}_1, x_{1\mathrm{r}}). \tag{17}$$

Notice that the product $\tilde{x}_1 \tilde{\rho}\big(\tilde{x}_1, x_{1\mathrm{r}}\big)$ is always positive given that function $\rho(\cdot)$ is strictly increasing, i.e., the function $\tilde{\rho}(\tilde{x}_1, x_{1\mathrm{r}})$ is positive when $\tilde{x}_1 = x_1 - x_{1\mathrm{r}} > 0$ and negative when $\tilde{x}_1 < 0$. Thus, the closed loop system (9) using the control signal (8), (14)

and the adaptive control law (11) is globally asymptotically stable.

IV. Practical Considerations

In this section some practical considerations regarding the previously derived control law are discussed.

A. Reference Computation

Notice that the control scheme derived in the previous section comprises expressions (6), (8), (11), and (14). From these expressions the most difficult to implement is (6), not only because it is a non-linear differential equation that requires to be solved numerically, but also because it needs either $x_{1\mathrm{r}}$ or $x_{2\mathrm{r}}$ as input argument. In order to tackle this inconvenience, a simpler expression equivalent to (6) has been obtained. Indeed, assuming that $x_{1\mathrm{r}}$ is a T_g-periodic signal, where T_g is the grid period, and integrating (6) over one grid period, yields,

$$A_{\mathrm{Ir}} = \frac{2}{AT_g}\int_{(n-1)T_g}^{nT_g}\Big(\hat{\Lambda}x_{1\mathrm{r}} - \rho(x_{1\mathrm{r}})x_{1\mathrm{r}}\Big)d\tau, \tag{18}$$

where $n \in \{1, 2, \ldots\}$. The aforementioned expression can be effortlessly solved if we take into account two easily verifiable assumptions, namely,

A1. L and C are chosen such that $x_{1\mathrm{r}} \approx \bar{x}_{1\mathrm{r}}$, where $\bar{x}_{1\mathrm{r}}$ is the average value of $x_{1\mathrm{r}}$,

A2. the solar irradiance and parameter Λ can be considered constant within one grid period $T_g = 20$ ms.

Given $x_{1\mathrm{r}}$ and the estimated value of $\hat{\Lambda}$, $x_{2\mathrm{r}}$ can be derived from (7) and (18) as

$$x_{2\mathrm{r}} = \frac{2\bar{x}_{1\mathrm{r}}\left(\hat{\Lambda} - \rho(\bar{x}_{1\mathrm{r}})\right)}{A}\sin(\omega t). \tag{19}$$

Figure 2 shows a block diagram of the proposed control scheme.

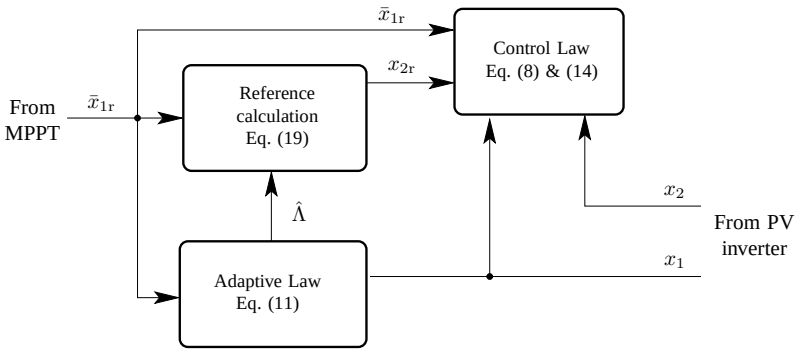

Fig. 2: Block diagram of the proposed non-liner control scheme.

B. Robustness

Even though the expressions that comprise the proposed controller depend on the system parameters, the closed-loop system presents some degree of robustness. This robustness is mainly due to the integral element present in the adaptive law (11) which forces $x_1 = \bar{x}_{1\mathrm{r}}$ and the possibility to neglect some of the control expression's terms that depend on the system parameters.

For instance, consider the case in which the inductance L is unknown and assume that $\hat{L} \neq L$ is the inductance used by the controller. With the following reference system,

$$\begin{aligned} C\dot{x}_{1\mathrm{r}} &= -u_{\mathrm{r}}\, x_{2\mathrm{r}} + \hat{\Lambda} - \rho(x_{1\mathrm{r}}) \\ \hat{L}\dot{x}_{2\mathrm{r}} &= u_{\mathrm{r}}\, x_{1\mathrm{r}} - v_g, \end{aligned} \tag{20}$$

the error dynamics (10) are modified as

$$\begin{aligned} C\dot{\tilde{x}}_1 &= -u_{\mathrm{r}}\, \tilde{x}_2 - \tilde{u}\,(x_{2\mathrm{r}} + \tilde{x}_2) + \tilde{\Lambda} - \tilde{\rho}(\tilde{x}_1, x_{1\mathrm{r}}) \\ \tilde{L}\dot{x}_{2\mathrm{r}} + (\hat{L} + \tilde{L})\dot{\tilde{x}}_2 &= u_r\, \tilde{x}_1 + \tilde{u}\,(x_{1\mathrm{r}} + \tilde{x}_1), \end{aligned} \tag{21}$$

where $\tilde{L} = L - \hat{L}$. Using the controllers defined by (8), (11), (14) and using the Lyapunov function (12) yields the following Lyapunov derivative

$$\dot{H} = -K\left(x_{1\mathrm{r}}\tilde{x}_2 - x_{2r}\tilde{x}_1\right)^2 - \tilde{x}_1\tilde{\rho}(\cdot) - \tilde{x}_2\tilde{L}\dot{x}_{2\mathrm{r}}, \tag{22}$$

which is the same as expression (17) but with an adding term depending on L, $\hat{L}$, x_2, $x_{2\mathrm{r}}$. Notice, however, that if $\tilde{x}_2$ is considered T_g-periodic, this adding term is bounded and the system remains BIBO (i.e., Bounded-Input Bounded-Output) stable. Moreover, if K is made sufficiently large the non-negative terms can dominate the positive component of (22).

Notice also that the contribution of the controller expression that contains the inductance in (8) can be neglected when

$$L\omega\; A_{\mathrm{Ir}}|_{\max(P_{\mathrm{pv}})} \ll A, \tag{23}$$

where $A_{\mathrm{Ir}}|_{\max(P_{\mathrm{pv}})}$ is the output current reference amplitude when the power generated by the PV array (P_{pv}) is maximum. Using (19) the aforementioned condition can be rewritten as

$$\max\left(P_{\mathrm{pv}}\right) \ll \frac{A^2}{2L\omega}, \tag{24}$$

which is valid in those cases where single-phase PV inverters are normally used, e.g., residential grid connected PV systems. For example, in the case of a 3 $\mathrm{kW_p}$ residential PV system connected to an European grid (i.e., $A = 312$ V) the expression with the inductance in (8) can be neglected if $L \ll 51$ mH. Figure 3 shows the numerical simulation results of the output current of a 3.25 $\mathrm{kW_p}$ grid-connected PV system using the single-phase inverter of Fig. 1 ($L = 2$ mH, $C = 2.2$ mF, $v_{\mathrm{g}} = 312\sin(100\pi t)$) and the proposed control scheme. Two cases have been simulated: one in which the complete expression of the controller is used and another one in which the term containing the inductance is neglected. Notice how the difference between both currents is unnoticeable.

With respect to the dependence of the proposed controller on the other system parameters the following remarks are in order:

R1. Equation (22) indicates that the closed-loop system is robust to any variation of Λ;

R2. Even though we do not consider any uncertainties in other system parameters, such as α and Ψ, in the theoretical analysis and derivation of the controller, the appearance of the integral term included for the estimation of Λ, i.e., the adaptive

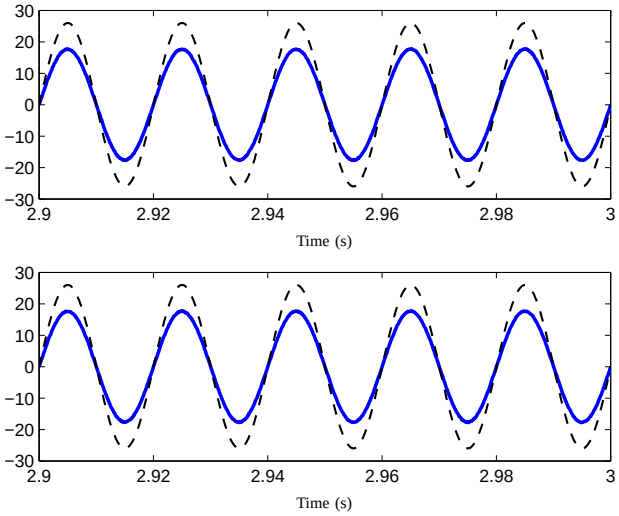

Fig. 3: Numerical simulation results of the output current for a 3.25 $\mathrm{kW_p}$ grid-connected PV system using the proposed controller with (top figure) and without (bottom figure) the term containing L. The scaled grid voltage, $v_\mathrm{g}/12$, is shown with dashed lines and its scale is in V, the other curve corresponds to x_2 in A.

law (11), adds a certain degree of robustness to possible uncertainties in the other system parameters.

Concerning R2, a series of numerical simulations have been performed in order to verify the robustness of our proposed controller in front of non-considered uncertainties, i.e., variations of α and Ψ. For the simulation we considered the system of Fig. 1 with $C = 2.2$ mF, $L = 2$ mH, $v_g = 312\sin(100\pi t)$ V and a PV array with a peak power of 3.3 kW, a short circuit current of 6.1 A, and a open circuit voltage of 678 V at 1000 W/m^2 ($\Lambda = 6.1$, $\alpha = 0.026$, $\Psi = 1.35 \times 10^{-7}$). The simulation tests consisted of two step-wise variations of α and Ψ of $+5\%$ and -5% at $t = 4$ s, where the average voltage reference value was set to 587.8 V. The simulation results are shown in Fig. 4 and Fig. 5, notice how in both cases the system is able to keep the commanded voltage value while maintaining at all time a sinusoidal current in phase with the grid voltage.

V. Experimental Tests

In order to test the designed control scheme under realistic conditions and further study its robustness in front of unmodeled dynamics a laboratory prototype was built. The schematic circuitry of the experimental prototype is shown in Fig. 6, where the signals x_1, x_2, and v_g enclosed in squares represent the measured capacitor voltage, inductor current and utility grid voltage, respectively. As an input energy source we used an Agilent E4350B Solar Array Simulator (SAS). This device enables to program different $i - v$ curves, which for experimental validation turns out to be very useful since it allows to generate fast changes in the PV array electrical characteristics. The $i-v$ curves programmed in the SAS for the experimental tests performed are shown in Fig. 7. Due to the solar array simulator low output voltage level (it has a maximum voltage of 80V), the GPV inverter prototype was connected to the grid by means of a step up transformer. All the measurements where done in the low-voltage side of the transformer which exhibits a voltage amplitude of 31.4 V at 50 Hz.

The controller implemented consisted of an analog circuitry in charge of dealing with an initial signal conditioning to assure that the measured signals stay within a given voltage level. The analog stage also generates the error signals, $\tilde{x}_1$ and $\tilde{x}_2$, and

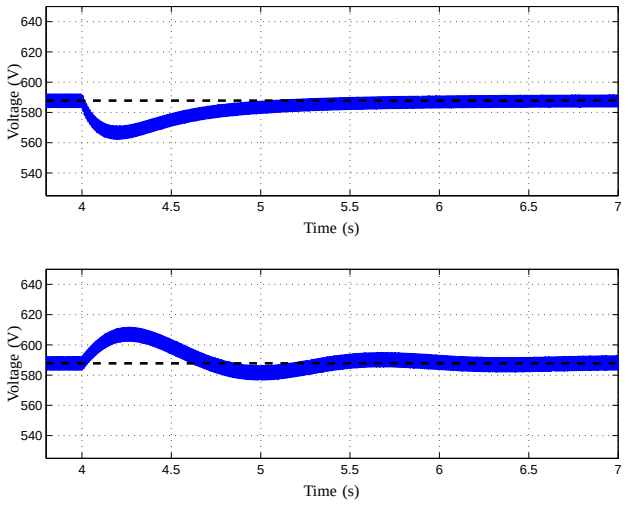

Fig. 4: Capacitor voltage: numerical simulation results of a $+5\%$ (top figure) and -5% (bottom figure) variation of α and Ψ. The variation of α and Ψ is done at $t = 4$ s. The dashed line represents the reference value.

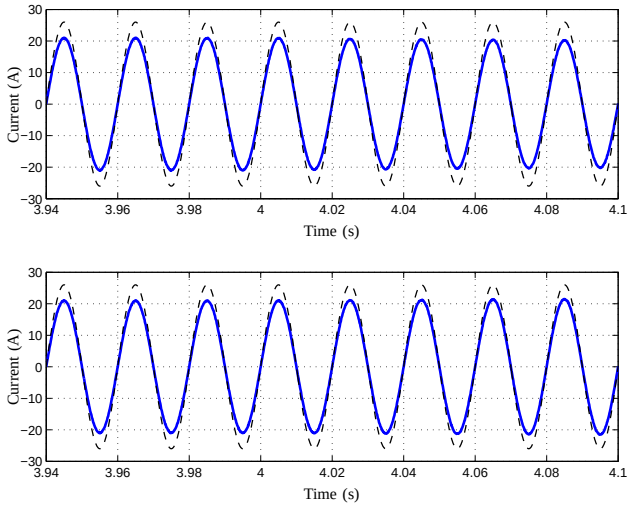

Fig. 5: Output current: numerical simulation results of a $+5\%$ (top figure) and -5% (bottom figure) variation of α and Ψ. The variation of α and Ψ is done at $t = 4$ s. The dashed line represents the scaled grid voltage ($v_g/12$).

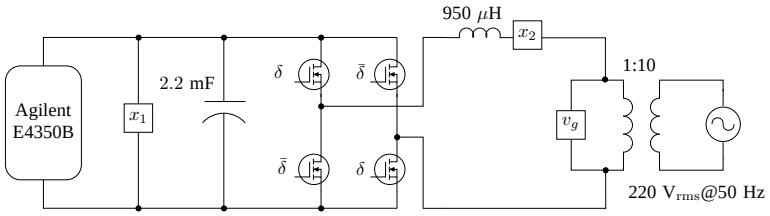

Fig. 6: Experimental Prototype Schematic Circuitry.

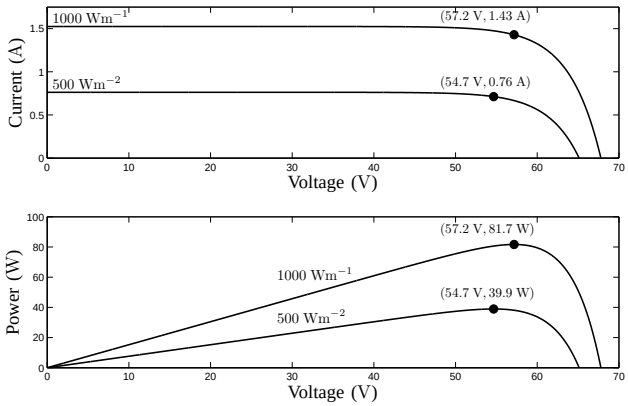

Fig. 7: PV array electrical curves used the experimental tests.

the derivative of x_2 in order to improve the dynamic range of the digital stage. The output signals of the analog module are then quantized by means of analog-to-digital (ADC) converters (ADC AD9525 of 12 bits and 25 MSPS). The quantized signals are then inputted to a digital processing stage implemented in a hardwired device, namely a Xilinx Spartan 3 field programmable gate array (FPGA). The hardwired algorithms implemented in the FPGA operates synchronously with a clock period of 4 ns. Additionally, the digital pulse width modulator (PWM) that generates the signals δ and $\bar{\delta}$ is implemented within the FPGA using a sawtooth carrier waveform with a period of 40.96 μs. Fig. 8 shows a block diagram of the experimental setup implemented, notice that as discussed in the previous section in order to simplify the controller $\bar{x}_{1\mathrm{r}}$ is used instead of $x_{1\mathrm{r}}$. Signal $\bar{x}_{1\mathrm{r}}$ is assumed to be given by an external MPPT. Fig. 9 shows the functions implemented in the FPGA.

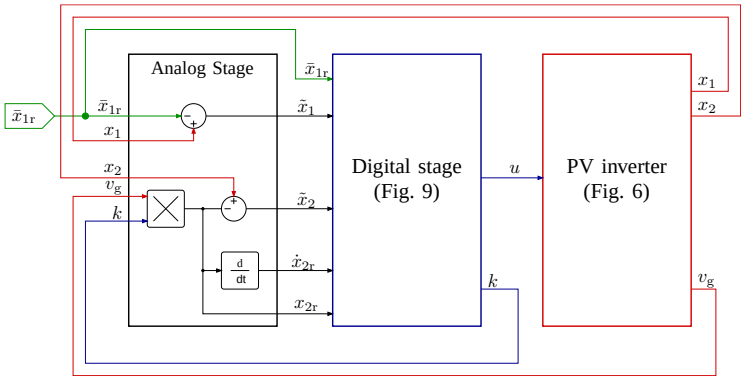

Fig. 8: Experimental prototype block diagram. Here k is a signal proportional to A_{Ir}, i.e., $k = \frac{A_{\mathrm{Ir}}}{A}$, see Fig. 9.

Two different experimental tests were performed:

T1. Experimental Test 1: This experimental test deals with the regulation of $\bar{x}_1$. The T_g-averaged reference value of the PV voltage, $\bar{x}_{1\mathrm{r}}$, is changed from 65 V to 61 V and finally arriving to the PV array maximum power point value (57.2 V), as it is graphically shown in Fig. 10. The reference value transitions were programmed to occur every 60 grid cycles, i.e., 1.2 s.

T2. Experimental Test 2: This test was designed to show the adequate behavior of the closed-loop GPV inverter when abrupt changes in the electrical characteristics of the solar array simulator occur, emulating sudden irradiance changes in the PV

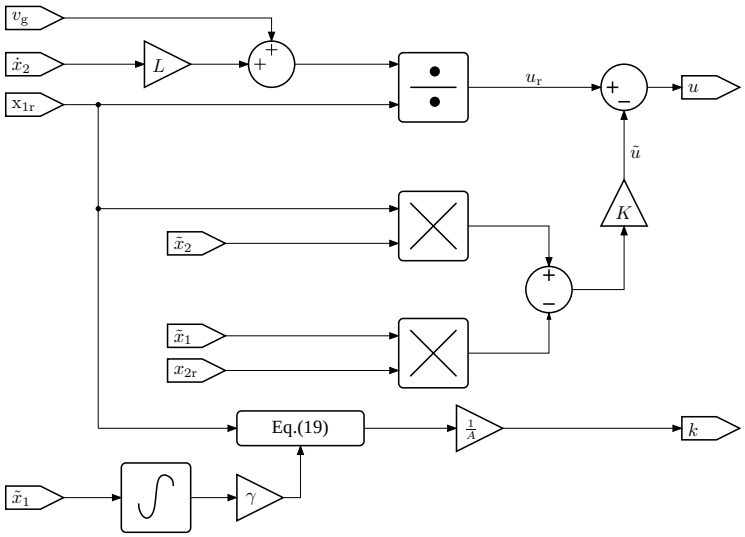

Fig. 9: Functions implemented in the FPGA.

array. The solar array simulator has been programmed with two set of electrical characteristics, one corresponding to an irradiance of $1000\ \mathrm{Wm}^{-2}$ and another corresponding to an irradiance of $500\ \mathrm{Wm}^{-2}$. The experimental test consisted in the sudden change of the $1000\ \mathrm{Wm}^{-2}$ electrical characteristics set to the $500\ \mathrm{Wm}^{-2}$ and then restoring the $1000\ \mathrm{Wm}^{-2}$ electrical characteristics set after a given time. This operation is shown in Fig. 11. This test is equivalent to an improvable worst case scenario and therefore it is a good way to validate the robustness of the designed controller.

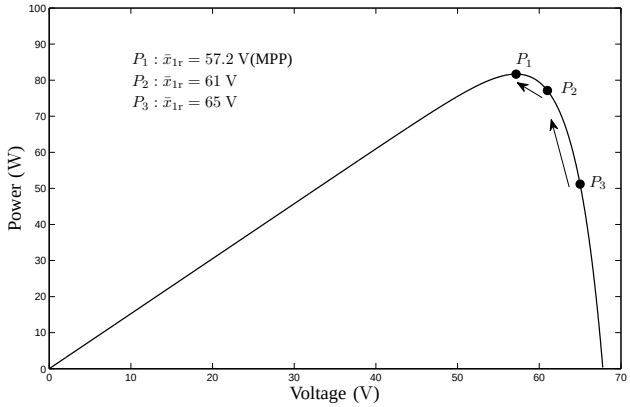

Fig. 10: Experimental Test 1.

The values of the tunable parameters of the controller, i.e., gains K and γ, have been defined mainly to avoid numerical problems (e.g., saturation of the signals, quantization problems). Therefore the gain K has been chosen as large as possible but avoiding saturation of signal u. The adaptive gain γ has been chosen such that a smooth non-oscillating x_1 dynamics is obtained. The final values of gains used were $K = 2.4$ and $\gamma = 0.05$.

Fig. 12 and Fig. 13 show the results of the aforementioned experimental tests. In the case of Experimental Test 1 (Fig. 12) it can be seen that the output current is always in phase with the grid voltage and that the capacitor voltage eventually reaches its desired steady-state value. The controller parameters have been intentionally set such that a smooth closed-loop voltage

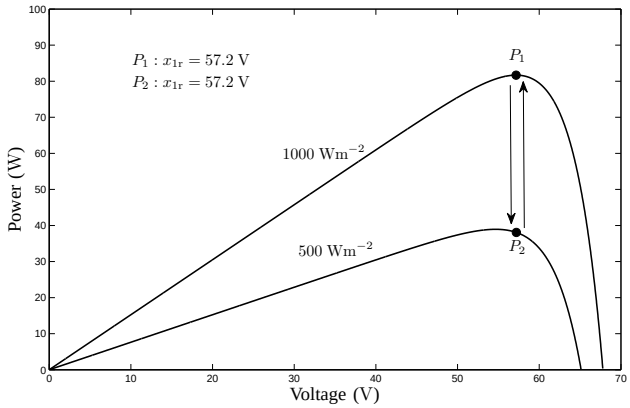

Fig. 11: Experimental Test 2.

dynamics is obtained in order to avoid the introduction of unwanted harmonics in the output current, i.e., in single-phase PV power inverters the effects of the voltage dynamics directly affects the output current.

Fig. 13 shows the electrical behavior of the full-bridge inverter prototype with the designed control scheme for Experimental Test 2. Notice that when the abrupt step-down irradiance change occurs ($t = 2.8$ s), after a settling time approximately equal to 0.3 s, the system is able to reach the desired steady state. A similar settling time is obtained when the step-up irradiance change occurs ($t = 7.05$ s). Note that during the complete experimental test the current injected to the utility grid is always in phase with the grid voltage. It should be remarked that the difference in the response of x_2 during the step-down and step-up irradiance change is due to the non-linear behavior of the system. The non-linear behavior becomes more apparent in the presence of large set-point changes, disturbances, or errors that cause the system to deviate from its nominal point of operation.

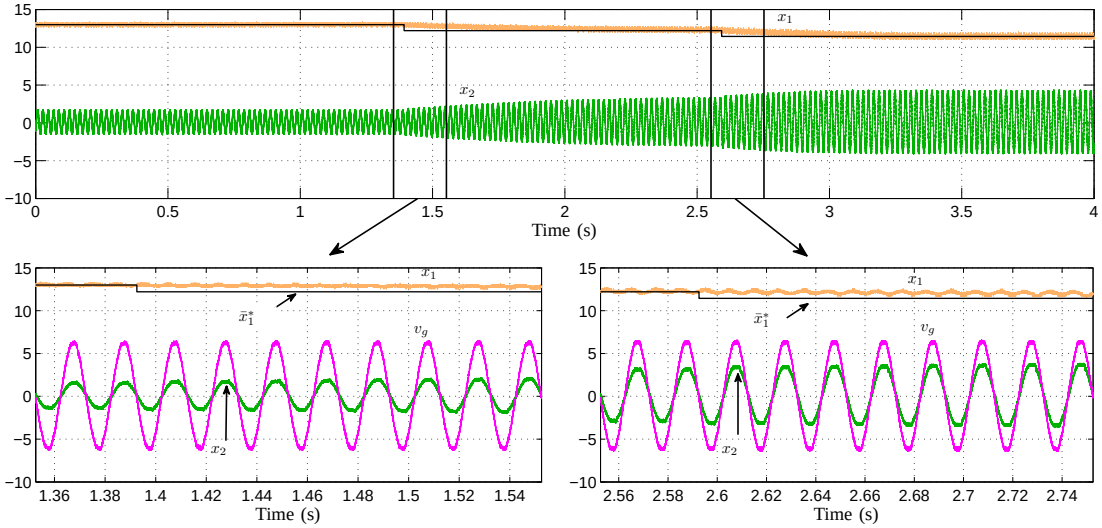

Fig. 12: Experimental Test 1. x_1, $\bar{x}_1^*$ and v_g at 5 V/div; x_2 at 1 A/div.

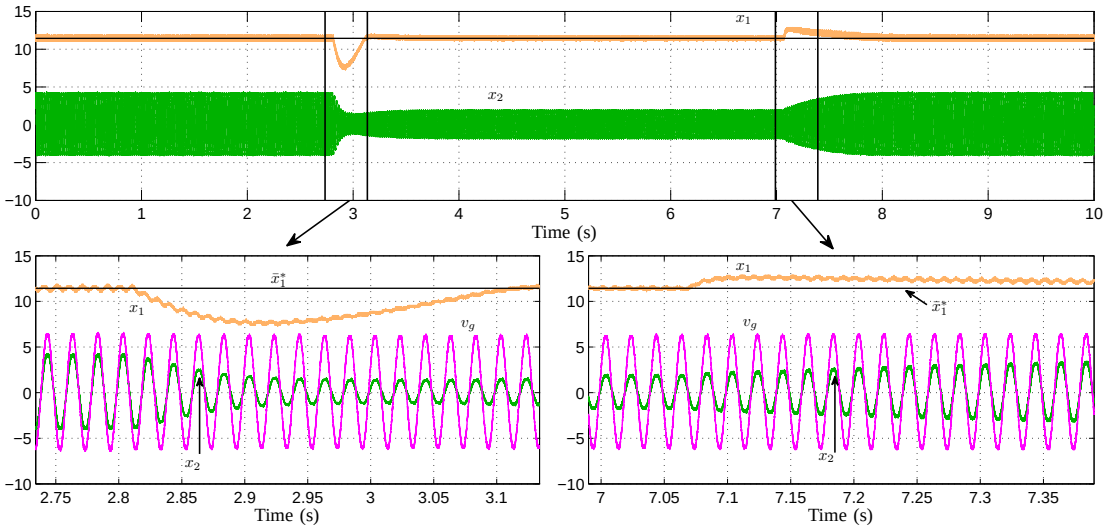

Fig. 13: Experimental Test 2. x_1, $\bar{x}_1^*$ and v_g at 5 V/div; x_2 at 1 A/div.

VI. Conclusions

A novel approach to the controller design for single-phase single-stage grid-connected power inverters is presented. Instead of linearizing the system, the control design approach aims to derive a global asymptotically stable closed-loop system that takes into account the non-linear time-varying characteristics of the system. The robustness of the controller has been improved by adding an adaptive control law. A further theoretical analysis of the closed-loop system supported by means of numerical simulations allows to simplify the implementation of the controller. A laboratory prototype was built in order to test the closed-loop performance of the controlled system. The experimental test performed consisted of an abrupt change of the PV array irradiance. Even though such sudden and large change is not likely to occur in reality, it serves to underscore the robustness and effectiveness of the proposed controller. The experimental results showed that the implemented controller was able to meet the desired control requirements, i.e., to extract a given amount of power from the PV array (Solar Array Simulator, in the case of the experimental prototype) and to inject to the utility grid a current in phase with the grid voltage—even under extreme changes in the system parameters.

The results of this paper should be considered as a proof of principle. It is expected that the proposed controller provides a similar performance as those obtained using standard linear controller design techniques. Moreover, the inclusion of the non-linear characteristics guarantees the closed-loop system to operate robustly and reliable, even in the presence of large set-point changes, disturbances, or errors that cause the system to deviate from its nominal point of operation. It is our believe that further research in the design and analysis of PV power systems considering and respecting their non-linear nature may help to obtain more efficient and reliable management and control algorithms than the ones currently available.

References

[1] G. Petrone, G. Spagnuolo, R. Teodorescu, M. Veerachary, and M. Vitelli, "Reliability issues in photovoltaic power processing systems," *IEEE Transaction on Industrial Electronics*, vol. 55, pp. 2569–2580, 2008.

[2] D. Zmood and D. Holmes, "Stationary frame current regulation of PWM inverters with zero steady-state error," *IEEE Transaction on Power Electronics*, vol. 18, pp. 814–822, May 2003.

[3] R. Teodorescu, F. Blaabjerg, M. Liserre, and P. C. Loh, "Proportional-resonant controllers and filters for grid-connected voltage-source converters," *IEE Transactions on Power Applications*, vol. 153, no. 5, pp. 750–762, September 2006 2006.

[4] R. Teodorescu, F. Blaabjerg, U. Borup, and M. Liserre, "A new control structure for grid-connected LCL PV inverters with zero steady-state error and selective harmonic compensation," in *Applied Power Electronics Conference and Exposition*, 2004.

[5] C.-Y. Chan, "A nonlinear control for DC-DC power converters," *IEEE Transactions on Power Electronics*, vol. 22, pp. 216–222, 2007.

[6] M. de Vries, M. Kransse, M. Liserre, V. Monopoli, and J. Scherpen, "Passivity-based harmonic control through series/parallel damping of an h-bridge rectifier," in *International Symposium on Industrial Electronics*. IEEE, 2007, pp. 3385–3390.

[7] D. Jeltsema and J. Scherpen, "A power-based perspective in modeling and control of switched power converters [past and present]," *IEEE Industrial Electronics Magazine*, vol. 1, pp. 7–54, 2007.

[8] A. Gensior, H. Sira-Ramirez, J. Rudolph, and H. Guldner, "On some nonlinear current controllers for three-phase boost rectifiers," *IEEE Transactions on Industrial Electronics*, vol. 56, pp. 360–370, 2009.

[9] S. Sanders and G. Verghese, "Lyapunov-based control for switched power converters," *IEEE Transactions on Power Electronics*, vol. 7, no. 1, pp. 17–24, January 1992.

[10] R. Leyva, A. Cid-Pastor, C. Alonso, I. Queinnec, S. Tarbouriech, and L. Martinez-Salamero, "Passivity-based integral control of a boost converter for large-signal stability," in *IEE Proceedings on Control Theory Applications*, 2006, pp. 139–146.

[11] H. Komurcugil and O. Kukrer, "A new control strategy for single-phase shunt active power filters using a Lyapunov function," *IEEE Transactions on Industrial Electronics*, vol. 53, no. 1, pp. 305–312, February 2006.

[12] C. Meza, D. Jeltsema, D. Biel, and J. Scherpen, "Passive P-control for grid-connected PV systems," in *17th IFAC World Congress*, 2008.

[13] G. Escobar, A. Stankovic, P. Mattavelli, F. Gordillo, and J. Aracil, "From adaptive PBC to PI nested control for SATCOM," in *IFAC Workshop on Digital Control*, IFAC, Ed., 2000.

[14] G. Escobar, D. Chevreau, R. Ortega, and E. Mendes, "An adaptive passivity-based controller for a unity power factor rectifier," *IEEE Transactions on Control Systems Technology*, vol. 9, no. 4, pp. 637–644, 2001.

[15] M. Calais, J. Myrzik, T. Spooner, and V. Agelidis, "Inverter for single-phase grid connected photovoltaic systems - an overview," in *Power Electronics Specialists Conference*, vol. 4. IEEE, February 2002, pp. 1995–2000.

[16] S. Kjaer, J. Pedersen, and F. Blaabjerg, "A review of single-phase grid-connected inverters for photovoltaic modules," *IEEE Transactions on Industry Applications*, vol. 41, no. 5, pp. 1292–1306, 2005.

[17] M. Meinhardt, "Past, present and future of grid connected photovoltaic and hybrid power systems," in *Power Engineering Society Summer Meeting*, vol. 2. IEEE, July 2000, pp. 1283–1288.

[18] S. Chiang, K. Chang, and Y. Yen, "Residential photovoltaic energy storage system," *IEEE Transactions on Industrial Electronics*, vol. 45, no. 3, pp. 385–394, 1998.

[19] D. Cruz-Martins and R. Demonti, "Photovoltaic energy processing for utility connected system," in *27th Annual Conferences of the IEEE Industrial Electronics Society*. IEEE, 2001.

[20] S. Busquets-Monge, J. Rocabert, P. Rodriguez, S. Alepuz, and J. Bordonau, "Multilevel diode-clamped converter for photovoltaic generators with independent voltage control of each solar array," *IEEE Transactions on Industrial Electronics*, vol. 55, no. 7, pp. 2713–2723, July 2008.

[21] C. Meza, J. Negroni, D. Biel, and F. Guinjoan, "Inverter configuration comparative for residential PV-grid connected systems," in *International Conference on Industrial Electronics*. IEEE, November 2006, pp. 4361–4366.

[22] J. Gow and C. Manning, "Development of a photovoltaic array model for use in power-electronics simulation studies," *Electric Power Applications, IEE Proceedings* -, vol. 146, no. 2, pp. 193–200, Mar 1999.

[23] S. Liu and R. Dougal, "Dynamic multi-physics model for solar array," *IEEE Transactions on Industrial Electronics*, vol. 17, no. 2, pp. 285–294, June 2002.

[24] U. Boke, "A simple model of photovoltaic module electric characteristics," in *European Conference on Power Electronics and Applications*, Sept. 2007, pp. 1–8.